Nuclear Instruments and Methods in Physics Research A 1069 (2024) 169847

Contents lists available at ScienceDirect

Nuclear Inst. and Methods in Physics Research, A

journal homepage: www.elsevier.com/locate/nima

A 350 GHz array of LEKIDs for balloon-borne CMB observations

F. Cacciotti [a,b,*], A. Paiella [a,b], C. Avestruz [c], R. Basu Tackur [d,e], E.S. Battistelli [a,b], P. de Bernardis [a,b], E. Bulbul [f], F. Columbro [a,b], A. Coppolecchia [a,b], S. Cray [g], G. D'Alessandro [a,b], M. De Petris [a,b], S. Hanany [g], L. Lamagna [a,b], E. Lau [h,i], S. Masi [a,b], G. Pettinari [j], F. Piacentini [a,b], J. Sayers [d], I. Zhuravleva [k], J. Zuhone [h]

[a] Physics Department, Sapienza University, Italy
[b] Istituto Nazionale di Fisica Nucleare, Sezione di Roma 1, Italy
[c] University of Michigan, USA
[d] California Institute of Technology, USA
[e] NASA Jet Propulsion Laboratory, USA
[f] Max Planck Institute for extraterrestrial Physics, Germany
[g] School of Physics and Astronomy, University of Minnesota, USA
[h] Harvard-Smithsonian Center for Astrophysics, USA
[i] Department of Physics, University of Miami, USA
[j] Istituto di Fotonica e Nanotecnologie - Consiglio Nazionale delle Ricerche, Italy
[k] Department of Astronomy and Astrophysics, University of Chicago, USA

ARTICLE INFO

Keywords:
OLIMPO
Kinetic inductance detector
Galaxy cluster

ABSTRACT

We present the design, optimization and laboratory characterization of an array of Lumped Element Kinetic Inductance Detectors sensitive in a frequency band centered at 350 GHz. The array consists of 313 feed-horn coupled pixels with resonant frequencies spread over 250 MHz. We present measured yield, quality factor, responsivity, quasiparticle lifetime, noise equivalent power and optical efficiency. The array is a prototype for one of the four frequency bands of OLIMPO, a balloon-borne instrument with a 2.6 m primary mirror proposed for an Antarctic flight to measure the Sunyaev–Zel'dovich effect in clusters of galaxies and their connecting filaments. Similar arrays could also be used with instruments studying the polarization of the cosmic microwave background radiation.

1. Introduction

Observations of clusters of galaxies in the millimeter wavelengths, in combination with X-ray observations, are of extreme importance to probe the dynamics of large-scale structures and to unveil the properties of the warm/hot intergalactic medium baryons [1]. OLIMPO, a multi-band, balloon-borne, 2.6 m primary mirror telescope, is proposed for its second flight from Antarctica, after the 2018 technological flight from Svalbard [2,3]. It is capable to map the microwave sky in the 145, 250, 350 and 460 GHz frequency bands with angular resolution spanning from $1'$ to $3.3'$ and a field of view of $24'$. Each of the four focal planes are equipped with an array of lumped element kinetic inductance detectors (LEKIDs), for a total of more than 1 thousand pixels cooled to the OLIMPO operating temperature of about 280 mK [4].

A KID [5] is a superconducting high-Q resonator that senses radiation when photons modify its kinetic inductance, producing a measurable shift of the resonant frequency. In this work, we showcase the dark performance of the 350 GHz band LEKIDs array, remarking the yield and the dark responsivity measured at the OLIMPO operating temperature.

2. Design and simulations

313 KIDs fit on a two inches diameter aberration-corrected focal plane, made of a 310 μm thick silicon wafer. The resonators are arranged on a triangular grid with 2.44 mm side, sampling the focal plane at $1/f\lambda$, where $1/f = 3$ is the OLIMPO focal ratio, maximizing the mapping speed of compact objects. KIDs are capacitively coupled to a single 50 Ω-matched microstrip feedline. Both the detectors and the feedline are made of 30 nm thick aluminum film, with a critical temperature of about 1.31 K. KIDs share the same absorber geometry: a IV order Hilbert curve whose absorption efficiency and spectra were optimized with electromagnetic simulation. Each resonator has a unique interdigitated

* Corresponding author at: Physics Department, Sapienza University, Italy.
E-mail address: federico.cacciotti@roma1.infn.it (F. Cacciotti).

https://doi.org/10.1016/j.nima.2024.169847
Received 30 June 2024; Received in revised form 21 August 2024; Accepted 4 September 2024
Available online 6 September 2024

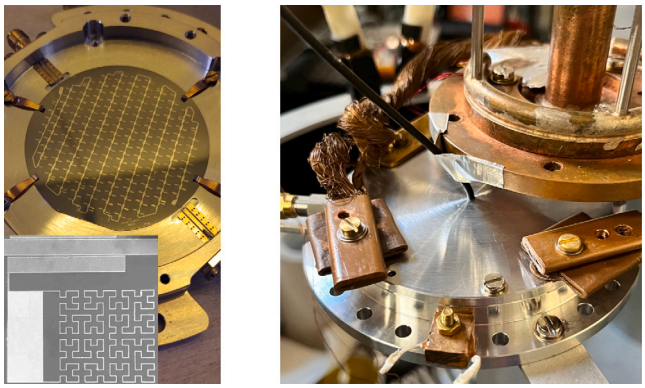

Fig. 1. Left panel: picture of the 350 GHz band KID array in its aluminum holder (credits G. Pettinari) and a close-up of a KID showing the absorber geometry, the IDC and the coupling capacitor. Right panel: the dark measurements setup showing the detector array holder on the sub-kelvin stage with an aluminum cap that ensures the minimal optical load. The black cable that reaches the center of the holder is an optical fiber used to send optical pulses to the central part of the wafer.

capacitor (IDC) and a microstrip coupling capacitor, which together with the inductor define the resonant frequency. An array of feedhorns and waveguides couples the KID array to the radiation [6]. A 200 nm metal layer covers the back of the wafer, ensuring both a ground reference and the backshort for the radiation to be detected. The array was fabricated at CNR-IFN [7] and is shown in the left panel of Fig. 1. A zoomed-in view of a KID shows the absorber geometry, the IDC, and the coupling capacitor with the feedline. The right panel of Fig. 1 shows the detector array holder on the sub-kelvin stage of our testbed.

The detector design was done in two steps: electromagnetic simulations using Ansys HFSS (to optimize the wafer size and material, the absorber geometry and absorption spectra and efficiency) and electric simulations using Sonnet (to define quality factors and resonant frequencies). Electrical simulations are briefly described in [8]. We managed to pack all the 313 detectors in about 250 MHz of readout bandwidth, with an average 0.7 MHz of frequency separation in agreement with the value of ≈0.8 MHz from simulations. We plan to use a 500 MHz wide readout bandwidth able to readout more than one array of KIDs for a total of about 500 detectors.

3. Dark measurements

Dark performance was measured using our dilution refrigerator testbed, able to reach a temperature of about 140 mK [9]. The detectors were subject to a minimal radiative load by enclosing them inside an aluminum holder. For different temperatures, we measured the quality factors, the resonant frequency and the electrical responsivity. KIDs are described by the complex transmission scattering parameter S_{21} defined as

$$S_{21} = 1 - \frac{Q_{tot}/Q_c}{1 + 2jQ_{tot}\delta x} \tag{1}$$

where j is the imaginary unit, $\delta x = (f - f_0)/f_0$ and f_0 is the KID resonant frequency. Q_{tot} is the total quality factor defined as

$$Q_{tot}^{-1} = Q_c^{-1} + Q_i^{-1} \tag{2}$$

where Q_c is the coupling quality factor and Q_i is the internal quality factor. The first takes into account energy losses due to electrical coupling effects with the feedline, while the latter depends on the quasiparticle number density, which changes with temperature.

We measured a detector yield, or the fraction of working detectors, of 92% at 140 mK. This number decreases to 85% at 280 mK because of resonance overlappings (whose resonant frequencies are separated by less than $\approx 5\nu_r/Q_{tot}$). The plot in Fig. 2 denotes the bias frequency

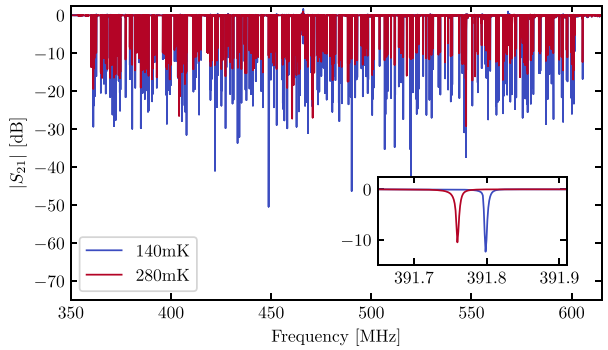

Fig. 2. Bias frequency sweep showing the S_{21} magnitude for the whole readout bandwidth. Red and blue lines outline the operating temperature. The inset plot shows a zoom on a resonance seen at the two temperatures.

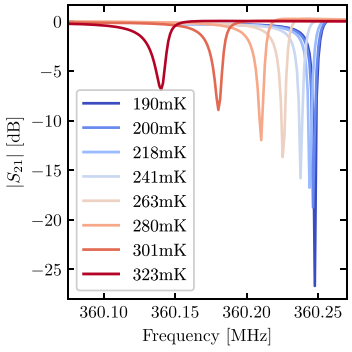

Fig. 3. Temperature sweep showing the amplitude of the S_{21} for one of the detectors. As the temperature rises the resonance became shallower and broader while shifting towards lower frequencies.

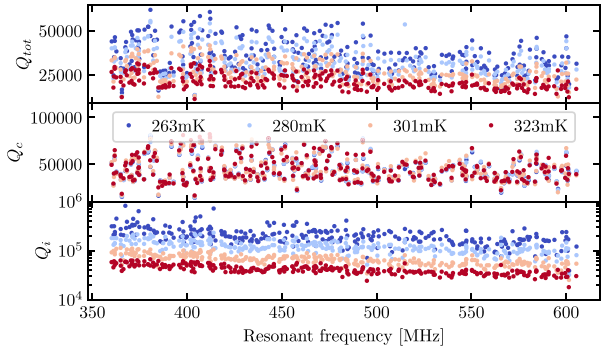

Fig. 4. Quality factors as a function of temperature and resonant frequency.

sweep at 140 mK and 280 mK, measured with a ROACH2 board.[1] The baseline of $|S_{21}|$ was subtracted flattening the frequency sweep. We measured the S_{21} for all the detectors at different temperatures as shown in Fig. 3.

A complex fit to Eq. (1) allows us to determine the quality factors for all the detectors at several temperatures, as shown in the plots in Fig. 4 as a function of the resonant frequency and for temperatures around the OLIMPO operating temperature.

As expected, Q_c does not depend on temperature while Q_i decreases as the temperature rises. The slight reduction of Q_i as the resonant frequency increases is due to a growth in the real part of the surface impedance of the superconducting material with frequency. This

[1] https://casper.astro.berkeley.edu/wiki/ROACH2.

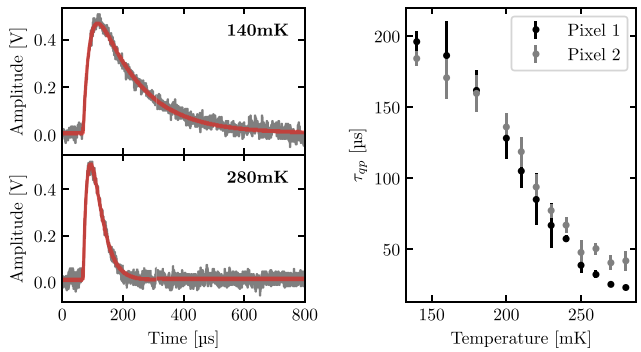

Fig. 5. Left panel: two cosmic ray events with the best fit curves in red, at two temperatures. Right panel: collection of τ_{qp} measurements at different temperatures for two representative resonators.

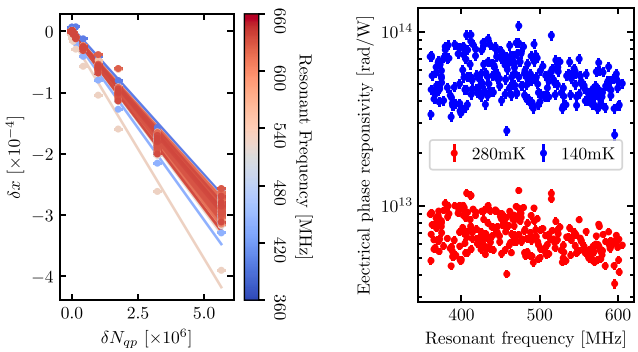

Fig. 6. Left panel: linear fit to the δx vs. δN_{qp} trend. Colorbar indicates the resonant frequency. Right panel: electrical phase responsivity as a function of the resonant frequency and temperature (blue is 140 mK and red is 280 mK).

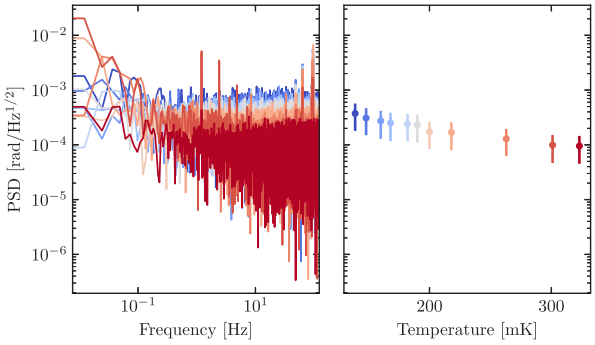

Fig. 7. Left panel: power spectral densities (PSDs) of a random detector at different temperatures between 140 mK (blue) and 320 mK (red). Right panel: average PSD around 10 Hz as a function of temperature.

growth is dominant with respect to the reduction in capacitance responsible for the increase in resonant frequency. The array average values for all the quality factors at the OLIMPO temperature of about 280 mK are in good agreement with the values predicted by simulations [8].

3.1. Quasiparticle lifetime

A quick and sudden pair-breaking energy injection such as cosmic ray events or μs-long light pulses produce glitches in the detector timestreams with a typical shape described by a finite impulse response function:

$$y(t) = A\left(e^{-t/\tau_{qp}} - e^{-t/\tau_r}\right) \tag{3}$$

where A is a constant amplitude, τ_r is the rise time and τ_{qp} is the quasiparticle lifetime. We measured τ_{qp} on a representative sample of detectors using a homodyne system with a 5 MHz sampling frequency. Both cosmic ray events and 650 nm light pulses were used to measure τ_{qp}. The plots on the left panel of Fig. 5 show two cosmic ray events for two temperatures and the best fit curves using Eq. (3). The right panel of Fig. 5 shows the behavior of τ_{qp} ($\sim n_{qp}(T)^{-1}$, where $n_{qp}(T)$ is the quasiparticle number density) with temperature for two representative KIDs. τ_{qp} is expected to reduce with increasing temperature: with an increase of quasiparticles in the superconductor, the recombination processes becomes more likely and then faster.

3.2. Electrical responsivity

Electrical responsivity is defined as

$$\mathcal{R}_{\phi,elec} = -\frac{4Q_{tot}\tau_{qp}}{\Delta}\frac{\delta x}{\delta N_{qp}} \tag{4}$$

where $\delta x = (\nu - \nu_r)/\nu_r$ is the dimensionless frequency shift and δN_{qp} is the change in thermal quasiparticle number, given by

$$N_{qp} = V_{abs} n_{qp}(T) \tag{5}$$

where $V_{abs} = 1101.60\,\mu m$ is the volume of the superconducting film. By making a linear fit to the δx vs. δN_{qp} (shown on the left panel of Fig. 6) and using the values for τ_{qp} found in 3.1 and the values for Q_{tot}, $\mathcal{R}_{\phi,elec}$ can be obtained (right panel of Fig. 6). We obtained an array average of $(56\pm15)\times10^{12}$ rad/W at 140 mK and $(6.9\pm1.6)\times10^{12}$ rad/W at 280 mK.

3.3. Noise

Noise spectra on the left panel of Fig. 7 clearly evidence the presence of two level system (TLS) noise at frequencies $\gtrsim 0.1$ Hz: increasing the temperature, the power spectral density (PSD) level gets lower. The TLS noise arises from lattice defects in the dielectric substrate that interact with the electric field of the resonators locally changing the relative dielectric constant. The plot on the right of Fig. 7 shows the average PSD at 10 Hz as a function of the temperature. The figure shows the noise level reaching a minimum plateau above ~270 mK.

TLS noise can be minimized by properly choosing the size and gaps of the KID capacitor, i.e. reducing the filling factor. This will result in wider capacitors and higher resonant frequency keeping the available surface fixed. The KID to KID separation of 2.44 mm is the limiting factor for the capacitor size. In the current design, the shape and size of capacitors were chosen such that the resonant frequencies span between ~350 MHz and ~600 MHz and the TLS contribution at 280 mK is lower. Smaller capacitors would have increased the resonant frequencies to the point that non-lumped electrical effects could have showed up.

4. Conclusions

In this contribution, we present the results of the electrical characterization of the 350 GHz KID array for the next-generation OLIMPO experiment. OLIMPO is a 2.6 m balloon-borne telescope intended to map clusters of galaxies in four photometric bands from Antarctica. We achieved an array yield of 92% at 140 mK and 85% at 280 mK. The analysis covered the quality factors, dark responsivity, quasiparticle lifetime, and noise characteristics of the array. The optical performance of this array is described in [8]. Overall, the characterization confirms that the 350 GHz KID array meets the design expectations, making it a viable candidate for precise cosmological observations with OLIMPO.

Declaration of competing interest

The authors declare that they have no known competing financial interests or personal relationships that could have appeared to influence the work reported in this paper.

References

[1] J. Sayers, et al., OLIMPO: A balloon-borne SZE imager to probe ICM dynamics and the WHIM, EPJ Web Conf. 293 (2024) 00049, http://dx.doi.org/10.1051/epjconf/202429300049.

[2] A. Paiella, et al., In-flight performance of the LEKIDs of the OLIMPO experiment, J. Low Temp. Phys. 199 (1–2) (2020) 491–501, http://dx.doi.org/10.1007/s10909-020-02372-y.

[3] S. Masi, et al., Kinetic Inductance Detectors for the OLIMPO experiment: in-flight operation and performance, J. Cosmol. Astropart. Phys. 2019 (07) (2019) 003, http://dx.doi.org/10.1088/1475-7516/2019/07/003.

[4] A. Coppolecchia, et al., The long duration cryogenic system of the OLIMPO balloon–borne experiment: Design and in–flight performance, Cryogenics 110 (2020) 103129, http://dx.doi.org/10.1016/j.cryogenics.2020.103129, URL: https://www.sciencedirect.com/science/article/pii/S0011227520301314.

[5] P.K. Day, et al., A broadband superconducting detector suitable for use in large arrays, Nature 425 (2003) 817, http://dx.doi.org/10.1038/nature02037.

[6] A. Paiella, et al., Kinetic inductance detectors for the OLIMPO experiment: design and pre-flight characterization, J. Cosmol. Astropart. Phys. 2019 (01) (2019) 039, http://dx.doi.org/10.1088/1475-7516/2019/01/039.

[7] A. Paiella, et al., Total power horn-coupled 150 GHz LEKID array for space applications, J. Cosmol. Astropart. Phys. 2022 (06) (2022) 009, http://dx.doi.org/10.1088/1475-7516/2022/06/009.

[8] F. Cacciotti, et al., Design and characterization of kinetic inductance detectors for the next-generation OLIMPO experiment, in: Millimeter, Submillimeter, and Far-Infrared Detectors and Instrumentation for Astronomy XII, Proc. SPIE 13102 (2024) 131020T, http://dx.doi.org/10.1117/12.3018300.

[9] S.J. Melhuish, et al., A tiltable single-shot miniature dilution refrigerator for astrophysical applications, Cryogenics 55–56 (2013) 63–67, http://dx.doi.org/10.1016/j.cryogenics.2013.03.002.